Sensors and Materials, Vol. 35, No. 2 (2023) 507–512
MYU Tokyo

S & M 3188

Synthesis of Lu_2O_3-Ga_2O_3-SiO_2 Glass as a New Glass Scintillator

Yuma Takebuchi,* Daiki Shiratori, Takumi Kato,
Daisuke Nakauchi, Noriaki Kawaguchi, and Takayuki Yanagida

Division of Materials Science, Nara Institute of Science and Technology (NAIST), Ikoma, Nara 630-0192, Japan

(Received September 26, 2022; accepted January 11, 2023)

Keywords: scintillator, glass, FZ method, radiation measurement

We synthesized $20Lu_2O_3$-$30Ga_2O_3$-$50SiO_2$ glasses doped with various concentrations of Sn using a floating zone furnace equipped with Xe arc lamps. The samples showed a luminescence band around 450 nm in both photoluminescence (PL) and scintillation spectra. The origin of the luminescence was ascribed to the T_1–S_0 transition of Sn^{2+} on the basis of the luminescence wavelength and PL decay time constant. The highest scintillation intensity and PL quantum yield were observed from the 1% Sn-doped sample. The afterglow level tended to decrease with increasing Sn doping, and the afterglow levels of the 1 and 3% Sn-doped samples were comparable to that of the conventional Tl-doped CsI scintillator. The optimal concentration of Sn for the glass was estimated to be 1%.

1. Introduction

A scintillator is a type of phosphor that can convert high-energy ionizing radiation into low-energy photons. The applications of scintillators are diverse, and they are used in medicine,[1] security,[2] and high-energy physics.[3] The main properties required for scintillators are a high light yield, short decay time, good energy resolution, low afterglow level, chemical stability, and suitable effective atomic number (Z_{eff}). No scintillator yet meets all of these requirements, and many researchers are investigating novel scintillators.[4–11] In the case of X- or γ-ray detection, the main interaction between the ionizing radiation and the scintillator is the photoelectric effect, and the cross section is proportional to the fifth power of Z_{eff}.[12] Therefore, a large Z_{eff} is important for high-energy X- or γ-ray detection. Although some commercial crystalline scintillators have a large Z_{eff},[13] the only commercial glass scintillator is ^{6}Li-glass (GS-20, Saint-Gobain), which is used for neutron detection and has a small Z_{eff} (Z_{eff} = 22.8).[14] Glass scintillators have several advantages over crystalline scintillators, such as a lower cost, a wider range of possible compositions, and better workability. However, glasses containing heavy elements (such as rare earths) often require melting at a high temperature of over 2000 °C. Therefore, the synthesis of a large-Z_{eff} glass is difficult using conventional techniques.

One of the solutions to this problem is the floating zone (FZ) method. This method was originally used for single-crystal growth;[15] however, we succeeded in applying it to glass

*Corresponding author: e-mail: takebuchi.yuma.ty1@ms.naist.jp
https://doi.org/10.18494/SAM4142

ISSN 0914-4935

synthesis.[16] The FZ method does not require a crucible, meaning the possibility of contamination from a crucible can be ignored. In addition, an FZ furnace equipped with Xe arc lamps can allow melting at high temperatures of up to 3000 °C.

In this study, we used Lu_2O_3-Ga_2O_3-SiO_2 glass as the host material. Since some Lu-containing crystalline scintillators including Lu_2SiO_5 and $Lu_2Si_2O_7$ have a large Z_{eff} and high light yield,[17–20] Lu_2O_3-SiO_2 glass is also expected to show good scintillation properties. Ga_2O_3 was predicted to play the role of an intermediate (network former) for this glass. Additionally, we added Sn to the host material as a luminescent center because some silicate glasses doped with Sn showed good luminescence properties.[21,22] In this study, we synthesized $20Lu_2O_3$-$30Ga_2O_3$-$50SiO_2$ glasses (Z_{eff} = 56.2) doped with Sn and evaluated their optical and scintillation properties.

2. Materials and Methods

We synthesized $20Lu_2O_3$-$30Ga_2O_3$-$50SiO_2$-xSnO (x = 0.1, 0.3, 1, and 3) glasses using an FZ furnace (FZ-T-12000-X-VPO-PC-YH, Crystal Systems Corporation) equipped with four Xe arc lamps. The starting materials were Lu_2O_3 (5N, Nippon Yttrium), Ga_2O_3 (4N, Furuuchi Chemical), SiO_2 (4N, Rare Metallic), and SnO (2N, High Purity Chemicals). The powders were mixed homogeneously and taken into a balloon to form a cylindrical rod by applying hydrostatic pressure The ceramic rods were sintered at 1200 °C for 8 h in air. Other details are explained in our previous report.[16] The only difference from our previous report was that the molten part was placed in a Pt crucible filled with water to quench it. Part of the obtained sample was polished by a polishing machine (Byehler, MetaServ 250), and the remaining part was crushed into a powder for powder X-ray diffraction (XRD) measurement. A diffractometer (Rigaku, MiniFlex600) was used for XRD.

Photoluminescence (PL) excitation and emission spectra and the PL quantum yield (QY) were measured using a Quantaurus-QY system (Hamamatsu Photonics, C11347). PL decay curves were measured using a Quantaurus-τ system (Hamamatsu Photonics, C11367) so as to obtain the PL decay time constants. Our original setup was used to measure scintillation spectra.[23] The scintillation intensity was compared using the scintillation spectra, taking into consideration differences in the sample weights. Afterglow profiles were obtained by an afterglow characterization system.[24] The afterglow level (ppm) was calculated as $1000000 \times (I_2 - I_{BG})/(I_1 - I_{BG})$, where I_{BG}, I_1, and I_2 are the background signal intensity, the signal intensity during X-ray irradiation, and the signal intensity obtained 20 ms after the irradiation was cut off, respectively.

3. Results and Discussion

Figure 1 shows the appearance of the samples. After polishing, each sample was approximately 3 mm long and 1 mm thick. The weights of the 0.1, 0.3, 1, and 3% Sn-doped samples were 64, 38, 25, and 43 mg, respectively. All samples were colorless and transparent and contained small cracks. The XRD patterns of the samples are shown in Fig. 2. Since a halo peak

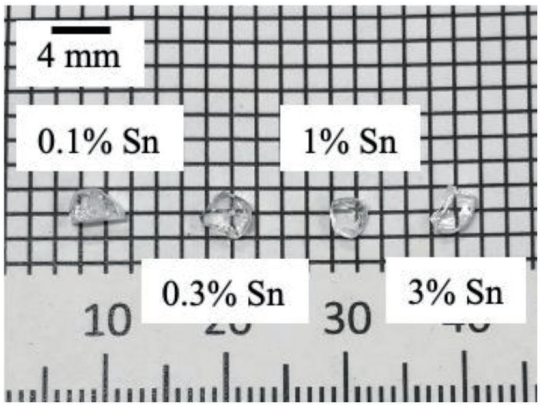

Fig. 1. Appearance of the synthesized samples.

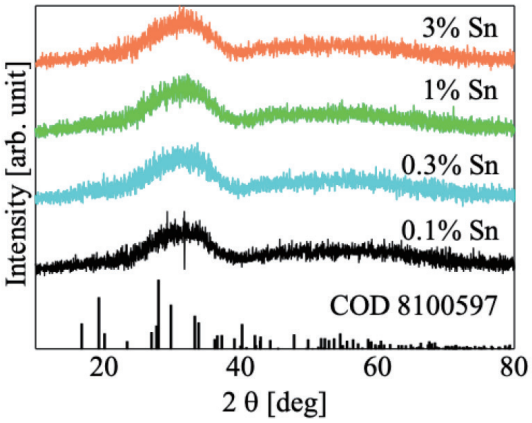

Fig. 2. (Color online) XRD patterns of the samples and reference of $Lu_2Si_2O_7$ (COD 8100597).

at 30° was observed, the synthesized samples were amorphous. The halo peak position corresponded to the reference pattern of $Lu_2Si_2O_7$ (COD 8100597). Therefore, the synthesized glasses may have formed a $Lu_2Si_2O_7$-like structure.[25]

Figure 3 depicts the PL excitation and emission spectra of the samples. A broad emission band was observed around 450 nm under excitation of around 300 nm. On the basis of the PL spectra and PL decay time constants (described later), the origins of the excitation and emission of the samples were ascribed to the S_0–S_1 and T_1–S_0 transitions of Sn^{2+}, respectively.[21,22,26] A redshift of the excitation band with increasing Sn concentration was observed. In a previous study, the reason for the redshift was given as follows. The S_1 band can be split into two different energy bands: higher and lower energy bands. Compared with the higher energy band, the lower energy band is more easily affected by the Sn concentration, with a redshift occurring with increasing Sn concentration.[27] The PL *QY* values of the 0.1, 0.3, 1, and 3% Sn-doped samples were 4.3, 7.0, 11.3, and 10.3%, respectively. A high PL *QY* of approximately 100% has been reported for some Sn-doped glasses, and the PL *QY* values of our samples were considerably lower.[21,27] Therefore, Sn^{4+}, which does not contribute to luminescence, might have been generated by oxidation and incorporated as a network former in the present samples.

Figure 4 shows the PL decay time profiles of the Sn-doped samples. The excitation and monitoring wavelengths were 280 and 450 nm, respectively. The decay curves were fitted with a single exponential decay function. The obtained decay time constants of the 0.1, 0.3, 1, and 3% Sn-doped samples were 5.06, 5.11, 5.13, and 5.12 μs, respectively, which are typical values for the T_1–S_0 transitions of Sn^{2+}.[22,27,28]

Figure 5 shows the scintillation spectra of the samples after correction for the weight of each sample. A broad emission band around 450 nm was observed for all the samples, similarly to in the PL spectrum. Thus, the origin of the luminescence was ascribed to the T_1–S_0 transition of Sn^{2+}. The highest scintillation intensity was detected from the 1% Sn-doped sample.

Figure 6 shows the afterglow profiles of the Sn-doped samples. The afterglow levels of the 0.1, 0.3, 1, and 3% Sn-doped samples were 1861, 1068, 390, and 422 ppm, respectively. The afterglow level tended to decrease with increasing Sn doping, and the afterglow levels of the 1

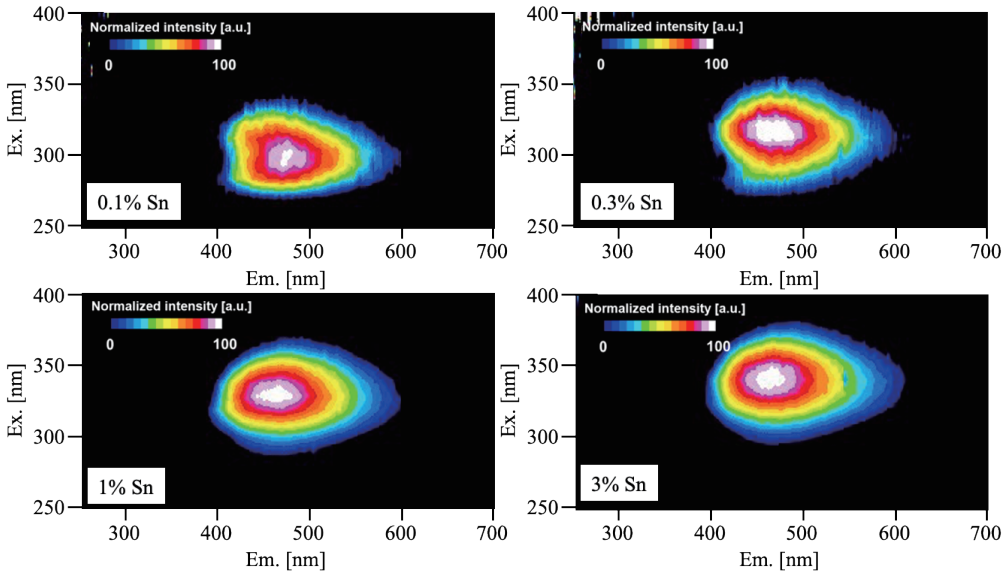

Fig. 3. (Color online) PL excitation and emission spectra of the samples.

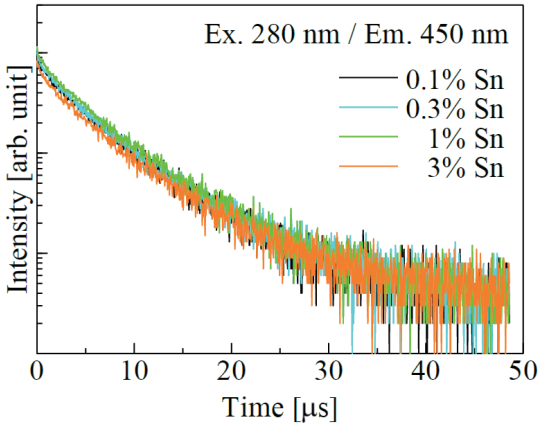

Fig. 4. (Color online) PL decay time profiles of the samples. The excitation and monitoring wavelengths were 280 and 450 nm, respectively.

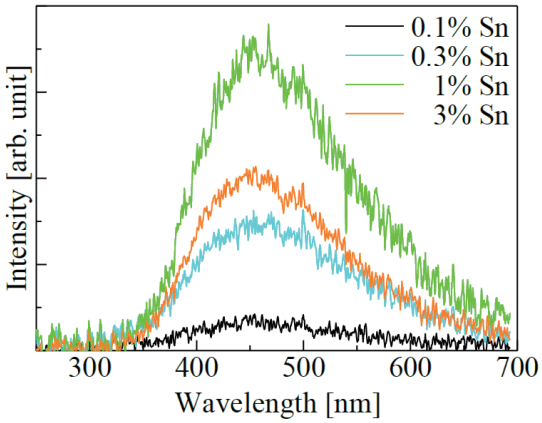

Fig. 5. (Color online) X-ray-induced scintillation spectra of the samples. The intensities were corrected for the weight of each sample.

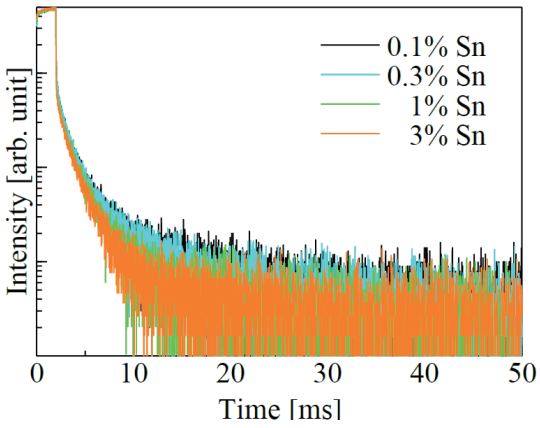

Fig. 6. (Color online) Afterglow profiles of the samples after 2 ms X-ray irradiation. The signal intensity was corrected for the background.

and 3% Sn-doped samples were comparable to that of the conventional Tl-doped CsI scintillator measured under the same condition.[29] Afterglow is a type of storage-type luminescence caused by shallow trapping centers and thermal stimulation at room temperature.[30,31] A low afterglow level indicates a small number of shallow trapping centers and high energy migration efficiency in the scintillation process. Generally, the scintillation efficiency is proportional to the energy migration efficiency and the luminescence efficiency (PL *QY*).[13] In this study, the trend of the scintillation intensity closely matched those of the PL *QY* and afterglow level. Therefore, the optimal Sn concentration for the $20Lu_2O_3$-$30Ga_2O_3$-$50SiO_2$ glass scintillator was estimated to be 1%.

4. Conclusions

We successfully synthesized $20Lu_2O_3$-$30Ga_2O_3$-$50SiO_2$ glasses doped with Sn using an FZ furnace equipped with Xe arc lamps. The XRD patterns of the samples indicated that they were amorphous and formed a $Lu_2Si_2O_7$-like structure. The PL and scintillation spectra showed luminescence at around 450 nm, and the PL decay time constant of the samples was approximately 5 μs, which is a typical value for the T_1–S_0 transition of Sn^{2+}. The highest PL *QY* and scintillation intensity were obtained from the 1% Sn-doped sample. The afterglow level tended to decrease with increasing Sn doping. The afterglow levels of the 1 and 3% Sn-doped samples were comparable to that of the conventional Tl-doped CsI scintillator. From the viewpoint of both the scintillation intensity and afterglow level, the optimal Sn concentration for the $20Lu_2O_3$-$30Ga_2O_3$-$50SiO_2$ glass was estimated to be 1%.

Acknowledgments

This work was supported by Grants-in-Aid for Scientific Research A (22H00309), B (21H03733, 21H03736, 22H02939, and 22H03872), Challenging Exploratory Research (22K18997), and JSPS Fellow (21J22668) from the Japan Society for the Promotion of Science. Foundation from Cooperative Research Project of the Research Center for Biomedical Engineering, Nippon Sheet Glass Foundation, Terumo Life Science Foundation, Iwatani Naoji Foundation, and Konica Minolta Science and Technology Foundation are also acknowledged.

References

1 C. W. E. van Eijk: Nucl. Instrum. Methods Phys. Res., Sect. A **509** (2003) 17. https://doi.org/10.1016/S0168-9002(03)01542-0
2 J. Glodo, Y. Wang, R. Shawgo, C. Brecher, R. H. Hawrami, J. Tower, and K. S. Shah: Phys. Procedia **90** (2017) 285. https://doi.org/10.1016/j.phpro.2017.09.012
3 R. Mao, L. Zhang, and R.-Y. Zhu: IEEE Trans. Nucl. Sci. **55** (2008) 2425. https://doi.org/10.1109/TNS.2008.2000776
4 T. Kunikata, T. Kato, D. Shiratori, D. Nakauchi, N. Kawaguchi, and T. Yanagida: Sens. Mater. **34** (2022) 661. https://doi.org/10.18494/SAM3683
5 M. Akatsuka, N. Daisuke, K. Takumi, N. Kawaguchi, and T. Yanagida: Sens. Mater. **34** (2022) 619. https://doi.org/10.18494/SAM3692

6 Y. Fujimoto, D. Nakauchi, T. Yanagida, M. Koshimizu, and K. Asai: Sens. Mater. **34** (2022) 629. https://doi.org/10.18494/SAM3693
7 T. Yanagida, T. Kato, D. Nakauchi, and N. Kawaguchi: Sens. Mater. **34** (2022) 595. https://doi.org/10.18494/SAM3684
8 K. Okazaki, D. Onoda, D. Nakauchi, N. Kawano, H. Fukushima, T. Kato, N. Kawaguchi, and T. Yanagida: Sens. Mater. **34** (2022) 575. https://doi.org/10.18494/SAM3678
9 R. Nakamori, N. Kawano, A. Takaku, D. Onoda, Y. Takebuchi, H. Fukushima, T. Kato, K. Shinozaki, and T. Yanagida: Sens. Mater. **34** (2022) 707. https://doi.org/10.18494/SAM3689
10 Y. Takebuchi, K. Watanabe, D. Nakauchi, H. Fukushima, T. Kato, N. Kawaguchi, and T. Yanagida: J. Ceram. Soc. Jpn. **129** (2021) 397. https://doi.org/10.2109/jcersj2.20233
11 H. Kimura, T. Kato, D. Nakauchi, N. Kawaguchi, and T. Yanagida: Sens. Mater. **34** (2022) 691. https://doi.org/10.18494/SAM3687
12 A. Phunpueok, V. Thongpool, and S. Jaiyen: J. Phys. Conf. Ser. **1380** (2019) 012128. https://doi.org/10.1088/1742-6596/1380/1/012128
13 T. Yanagida: Proc. Japan Acad. Ser. B **94** (2018) 75. https://doi.org/10.2183/pjab.94.007
14 V. Popov and P. Degtiarenko: IEEE Nucl. Sci. Symp. Med. Imaging Conf. (IEEE, 2010) 1819. https://doi.org/10.1109/NSSMIC.2010.5874089
15 S. M. Koohpayeh, D. Fort, and J. S. Abell: Prog. Cryst. Growth Charact. Mater. **54** (2008) 121. https://doi.org/10.1016/j.pcrysgrow.2008.06.001
16 D. Shiratori, D. Nakauchi, H. Fukushima, T. Kato, N. Kawaguchi, and T. Yanagida: Opt. Mater. **105** (2020) 109895. https://doi.org/10.1016/j.optmat.2020.109895
17 C. L. Melcher and J. S. Schweitzer: IEEE Trans. Nucl. Sci. **39** (1992) 502. https://doi.org/10.1109/23.159655
18 D. Pauwels, N. Le Masson, B. Viana, A. Kahn-Harari, E. V. D. van Loef, P. Dorenbos, and C. W. E. van Eijk: IEEE Trans. Nucl. Sci. **47** (2000) 1787. https://doi.org/10.1109/23.914446
19 P. Kantuptim, H. Fukushima, H. Kimura, D. Nakauchi, T. Kato, M. Koshimizu, N. Kawaguchi, and T. Yanagida: Sens. Mater. **33** (2021) 2195. https://doi.org/10.18494/SAM.2021.3316
20 P. Kantuptim, D. Nakauchi, T. Kato, N. Kawaguchi, and T. Yanagida: Sens. Mater. **34** (2022) 603. https://doi.org/10.18494/SAM3690
21 D. Shiratori, H. Kimura, D. Nakauchi, T. Kato, N. Kawaguchi, and T. Yanagida: Radiat. Meas. **134** (2020) 106297. https://doi.org/10.1016/j.radmeas.2020.106297
22 H. Fukushima, D. Shiratori, D. Nakauchi, T. Kato, N. Kawaguchi, and T. Yanagida: Sens. Mater. **34** (2022) 717. https://doi.org/10.18494/SAM3691
23 T. Yanagida, K. Kamada, Y. Fujimoto, H. Yagi, and T. Yanagitani: Opt. Mater. **35** (2013) 2480. https://doi.org/10.1016/j.optmat.2013.07.002
24 T. Yanagida, Y. Fujimoto, T. Ito, U. Kor, and K. Mori: Appl. Phys. Express **7** (2014) 6. https://doi.org/10.7567/APEX.7.062401
25 Z. Shi, S. Zhou, and Z. Yang: J. Am. Ceram. Soc. **104** (2021) 2030. https://doi.org/10.1111/jace.17643
26 Z. Hua, G. Tang, Q. Wei, P. Cai, L. Qin, S. Qian, and Z. Wang: Opt. Mater. **125** (2022) 112102. https://doi.org/10.1016/j.optmat.2022.112102
27 H. Masai, T. Tanimoto, T. Fujiwara, S. Matsumoto, Y. Tokuda, and T. Yoko: Opt. Express **20** (2012) 27319. https://doi.org/10.1364/OE.20.027319
28 M. Leskelä, T. Koskentalo, and G. Blasse: J. Solid State Chem. **59** (1985) 272. https://doi.org/10.1016/0022-4596(85)90294-4
29 K. Takahashi, H. Kimura, D. Nakauchi, T. Kato, N. Kawaguchi, and T. Yanagida: Jpn. J. Appl. Phys. **59** (2020) 102002. https://doi.org/10.35848/1347-4065/abb5c0
30 A. Luchechko, Y. Zhydachevskyy, S. Ubizskii, O. Kravets, A. I. Popov, U. Rogulis, E. Elsts, E. Bulur, and A. Suchocki: Sci. Rep. **9** (2019) 9544. https://doi.org/10.1038/s41598-019-45869-7
31 N. Kawano, K. Shinozaki, T. Kato, D. Onoda, Y. Takebuchi, H. Fukushima, and T. Yanagida: J. Lumin. **249** (2022) 119003. https://doi.org/10.1016/j.jlumin.2022.119003